ACS APPLIED MATERIALS & INTERFACES

Research Article

www.acsami.org

Free-Standing Three-Dimensional Graphene/Manganese Oxide Hybrids As Binder-Free Electrode Materials for Energy Storage Applications

Xiaoli Zhu,[†,∥,⊥] Peng Zhang,[†,∥,⊥] Shan Xu,[§] Xingbin Yan,[*,†,‡] and Qunji Xue[‡]

[†]Laboratory of Clean Energy Chemistry and Materials, Lanzhou Institute of Chemical Physics, Chinese Academy of Science, Lanzhou 730000, People's Republic of China

[‡]State Key Laboratory of Solid Lubrication, Lanzhou Institute of Chemical Physics, Chinese of Academy of Sciences, Lanzhou 730000, People's Republic of China

[§]State Key Laboratory for Oxo Synthesis and Selective Oxidation, Lanzhou Institute of Chemical Physics, Chinese Academy of Sciences, Lanzhou 730000, People's Republic of China

[∥]Graduate University of Chinese Academy of Sciences, Chinese of Academy of Sciences, Beijing 100080, People's Republic of China

Supporting Information

ABSTRACT: Novel three-dimensional (3D) hybrid materials, i.e., free-standing 3D graphene-supported MnO_2 nanosheets, are prepared by a simple and controllable solution-phase assembly process. Characterization results show that MnO_2 nanosheets are uniformly anchored on a 3D graphene framework with strong adhesion and the integral hybrids show desirable mechanical strength. Such unique structure of 3D graphene/MnO_2 hybrids thus provides the right characteristics of binder-free electrode materials and could enable the design of different kinds of high-performance energy storage devices. Especially, an advanced asymmetric supercapacitor is built by using a 3D graphene/MnO_2 hybrid and a 3D graphene as two electrodes, and it is able to work reversibly in a full operation voltage region of 0−3.5 V in an ionic liquid electrolyte and thus exhibits a high energy density of 68.4 Wh/kg. As the cathode materials for Li−O_2 and Li−MnO_2 batteries, the 3D graphene/MnO_2 hybrids exhibit outstanding performances, including good catalytic capability, high reversible capacity and desirable cycling stability. The results presented here may pave a way for new promising applications of such 3D graphene/MnO_2 hybrids in advanced electrochemical energy storage devices.

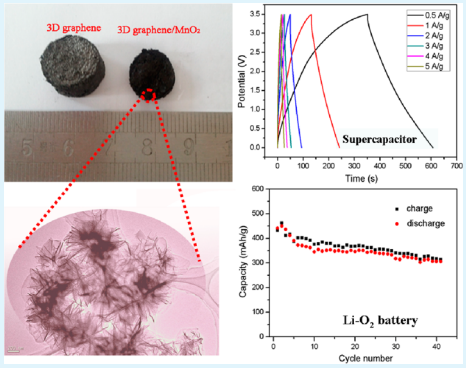

KEYWORDS: *3D graphene, MnO_2, supercapacitor, Li−O_2 battery, Li−MnO_2 battery*

1. INTRODUCTION

Recently, three-dimensional (3D) graphene, a framework of connecting graphene sheets, has attracted great interest in energy applications due to its ultrahigh surface-to-volume ratio, high porosity, strong mechanical strength, excellent electrical conductivity and fast mass and electron transport kinetics.[1−3] For instance, 3D graphene has been successfully applied in various electrochemical energy storage devices, such as supercapacitors,[4−6] Li-ion batteries,[7] Li−O_2 batteries,[8] Li−S batteries[9] and fuel cells.[10] However, these reported devices, using single 3D graphene, are mostly not capable of providing the sufficient energy density (for supercapacitors) or a satisfactory catalytic property (for Li−O_2 batteries, etc.). To remedy this problem, one effective strategy is to prepare the hybrids by combining 3D graphene with nanostructural metal oxides (MOs). The presence of MOs is able to efficiently prevent the aggregation of graphene sheets, consequently leading to an increase of the available electrochemical active area for energy storage.[11] More importantly, MOs exhibit much higher theoretical specific capacitance (MOs can undergo reversible redox reactions on/and within their thin surface layers) and much better catalytic performance than passive carbon materials.[12,13] Up to now, various 3D graphene/MOs hybrids, such as 3D graphene/$Ni(OH)_2$,[12] 3D graphene/Co_3O_4,[14] 3D graphene/FeO_x,[15] 3D graphene/MoS_2[16] and 3D graphene/MnO_2,[11] have been prepared, and they have showed that the incorporation of MOs into the 3D graphene framework has the potential to take advantage of both components to achieve greatly improved overall performance.

Among numerous MOs, MnO_2 is one of the most attractive candidates as an electrode material owning to its outstanding electrochemical properties combined with abundant natural resources, low-cost and environmental friendliness. In the supercapacitors aspect, 3D graphene/MnO_2 hybrids have been recently used as the electrode materials of aqueous supercapacitors

Received: April 23, 2014
Accepted: June 30, 2014
Published: June 30, 2014

(ASs). For example, Huh et al. reported an AS assembled by using 3D MnO_2/e-CMG (embossed-chemical modified graphene) and e-CMG showing a high energy density of 44 Wh/kg.[11] Wang et al. prepared an AS based on 3D porous graphene/MnO_2 nanorods and graphene/Ag hybrid, which exhibited a maximum energy density of 50.8 Wh/kg.[17] Xie et al. reported a 3D graphene/CNT/MnO_2 based AS having a maximum energy of 33.71 Wh/kg.[18] However, the potential windows of these ASs are limited in the range of 0−2 V due to the low decomposition potential of water, resulting in the still unsatisfactory energy density. In the rechargeable Li batteries aspect, powdery graphene/MnO_2 hybrids have been receiving intense interest because they are promising cathode materials for Li−O_2 and Li−MnO_2 batteries. For example, Dong et al. reported that the Li−O_2 battery using α-MnO_2/graphene nanosheets as a cathode material displayed excellent catalytic performance.[13] Liu et al. utilized MnO_2 nanorods/graphene composite in Li−MnO_2 battery and obtained a high initial discharge capacity of 241 mAh/g at 0.1 C and good cycling stability.[19] However, the studies on the 3D graphene/MnO_2 hybrids for Li−O_2 and Li−MnO_2 batteries are very limitedly reported.

In this paper, free-standing 3D graphene/MnO_2 hybrids are prepared by solution-phase deposition of MnO_2 nanosheets onto the 3D graphene framework. The highly conductive networks of graphene framework, strong adhesion between MnO_2 and graphene and desirable mechanical strength of the integral hybrid enable the as-made 3D graphene/MnO_2 hybrids can be directly served as the binder-free electrodes without any need for the additives. They can be used for designing different energy storage devices. For instance, an asymmetric supercapacitor based on a 3D graphene/MnO_2 hybrid and a 3D graphene is built, and it exhibits a wide voltage window of 3.5 V and a high energy density of 68.4 Wh/kg in 1-ethyl-3-methylimidazolium tetrafluoroborate/acetonitrile (EMIMBF_4/AN) ionic liquid electrolyte. To the best of our knowledge, it is the first time to investigate the electrochemical capacitive properties of 3D graphene/MnO_2 hybrid in a given ionic liquid electrolyte. Moreover, as the cathode materials, the 3D graphene/MnO_2 hybrids exhibit superior catalytic performance with the medium voltage difference as low as 0.75 V at 50 mA/g in a Li−O_2 battery, and display outstanding cycle performance in Li−O_2 and Li−MnO_2 batteries.

2. EXPERIMENTAL SECTION

2.1. Synthesis of 3D Graphene. In a typical preparation, graphene oxide (GO) was prepared from natural graphite by a modified Hummers method.[20] GO dispersion (3 mg/mL, 30 mL) was mixed uniformly with 120 μL of ethylenediamine (EDA) by sonication for 5 min. The resulting stable suspension was transferred into a 50 mL Teflon-lined autoclave and heated for 6 h at 120 °C for the synthesis of the 3D graphene hydrogel.[3] After the subsequent freeze-drying, the 3D graphene aerogel was produced.

2.2. Synthesis of 3D Graphene/MnO_2 Hybrids. First, the 3D graphene aerogel (30 mg) was cut into thin pellicles. Second, $KMnO_4$ (100 mg) was dispersed in 30 mL of deionized water and the solution was heated to 80 °C in an oil bath. The pH of the solution was adjusted to 2 by adding 2 M HCl(aq). To prepare 3D graphene/MnO_2 hybrids, each 3D graphene pellicle was added into the $KMnO_4$ solution and kept at 80 °C for different times (10, 30, 60 or 120 min) and then washed with deionized water and dried at 100 °C overnight. The final samples were respectively denoted as 3D graphene/MnO_2-x (x = 10, 30, 60 or 120).

2.3. Morphology and Structural Characterization. Scanning electron microscopy (SEM) analyses were performed with a field emission scanning electron microscope (JEOL-6701F) at an acceleration voltage of 5 kV. Transmission electron microscopy (TEM) investigations were conducted on a JEOL 2100 FEG microscope at 200 keV. To investigate the structure and composition of the samples, X-ray diffraction (XRD) patterns were characterized on a powder X-ray diffraction system (TTR-III) using Cu Kα radiation, and Raman spectra were measured on a Raman spectrometer (Lab RAMHR800, Horiba, Hobin Yvon) using 532 nm laser excitation. The chemical species of the as-prepared 3D graphene/MnO_2 hybrids were examined by a X-ray photoelectron spectroscope (XPS, Physical Electronics, PerkinElmer PHI-5702) with 1486.6 eV radiation as the excitation source. All the XPS spectra were calibrated by using Au $4f_{7/2}$ at 84.0 eV. The content of MnO_2 phase in each 3D graphene/MnO_2 hybrid was also analyzed by XPS and Elements analyzer (EA, VarioEL, for detecting C, N and O). The nitrogen adsorption−desorption isotherm measurements were performed on a Micromeritics ASAP 2020 M volumetric adsorption analyzer at 77 K. The Brunauer−Emmett−Teller (BET) method was utilized to calculate the specific surface area.

2.4. Electrochemical Measurements. Supercapacitor. The working electrodes were prepared as follows: each as-prepared 3D graphene or 3D graphene/MnO_2 pellicle (the mass was 0.5 mg) was directly pressed onto a nickel foam (1.5 × 1.5 cm) by physical pressing (15 MPa). Electrochemical measurements were carried out using an electrochemical working station (CHI660D, Shanghai, China) at room temperature in a closed three-electrode system with a saturated calomel electrode as the reference electrode and a platinum gauze electrode as the counter electrode. The electrochemical impedance spectrum (EIS) measurement was performed in the frequency ranging from 100 kHz to 0.05 Hz at 0.25 V with an AC perturbation of 5 mV. The average specific capacitance was calculated from the galvanostatic discharge curve, using the following equation:

$$C = I/[(\mathrm{d}V/\mathrm{d}t)m] \approx I/[(\Delta V/\Delta t)m](F/g) \quad (1)$$

where I is the constant discharge current (A), Δt is the discharge time (s), m is the mass of the corresponding active electrode material (g) and ΔV is the voltage change after a full discharge (V).

A two-electrode cell configuration was used to measure the performance of as-made AS in 2 M EMIMBF_4/AN electrolyte. To construct the AS, the 3D graphene pellicle (0.7 mg) and the 3D graphene/MnO_2-60 pellicle (0.3 mg) were used as the negative electrode and the positive electrode, respectively. Their mass ratio was decided based on charge balance theory ($q^+ = q^-$).[21,22] For building a cell, in a glovebox filled with argon, two electrodes separated by a porous nonwoven cloth separator were pressed together and assembled into a coin cell (2032 style). After the EMIMBF_4/AN electrolyte was injected, the cell was covered by pressure. The energy density (E) of AS was calculated by the specific capacitance (C) and the cell voltage (V) according to the following equation:

$$E = 0.5CV^2(\mathrm{Wh/kg}) \quad (2)$$

The power density (P) of AS was achieved by the E and the discharging time (t) according to the following equation:

$$P = E/t(\mathrm{W/kg}) \quad (3)$$

Li−O_2 Battery. The 3D graphene or the 3D graphene/MnO_2 pellicle (0.5 ± 0.15 mg) was directly used as the O_2 electrode without grinding or adding any additives. The battery assembly was operated in a glovebox filled with pure argon. The two electrodes (the anode electrode was a metallic Li foil) were separated by a separator (celgard 2400) dipping with 1 M $LiCF_3SO_3$ in tetraethylene glycol dimethyl ether−lithiumtriflate (TEGDME). This Li foil/separator/O_2 electrode sandwich was then sealed into a coin cell with 20 air holes (1 mm diameter) on the positive electrode side to flow oxygen. All the cells were tested using a LAND testing system (CTA2001A, Wuhan Land Electronic Co. Ltd.). All experiments were carried out in high-purity oxygen atmosphere, and the specific capacity was calculated based on the weight of 3D graphene or 3D graphene/MnO_2.

Li−MnO_2 Battery. The 3D graphene/MnO_2-120 pellicle (0.5 ± 0.15 mg) was directly used as the positive electrode without grinding or pressing. It was assembled into a coin cell (CR2032) in an argon-filled glovebox using 1 M $LiPF_6$ in ethylenecarbonate (EC) and dimethyl

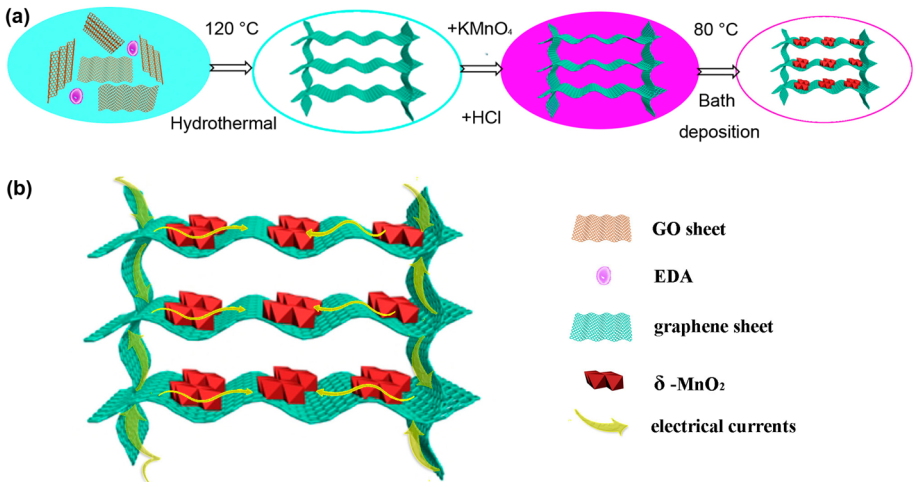

Figure 1. (a) Schematic illustration of the preparation of 3D graphene/MnO_2 hybrid, and (b) illustrations of electrons transfer on 3D graphene/MnO_2 hybrid.

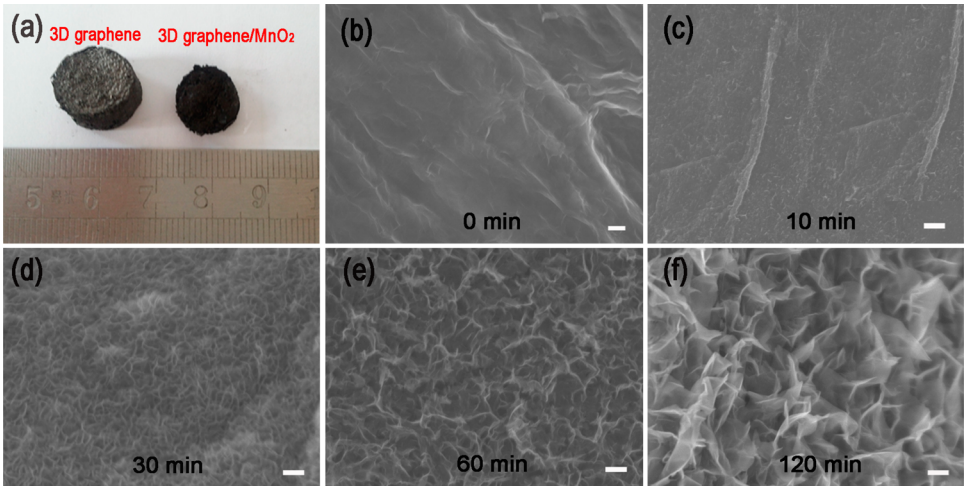

Figure 2. (a) Photographs of 3D graphene (left) and 3D graphene/MnO_2 hybrid (right) architectures. Typical SEM images of the 3D graphene/MnO_2 hybrids prepared at 80 °C with different deposition times: (b) 0, (c) 10, (d) 30, (e) 60 and (f) 120 min. Scale bar, 100 nm.

carbonate (DMC) (1:1, v/v) as the electrolyte and Li foil as the counter electrode, and the celgard 2400 membrane as the separator. The assembled coin cell was tested in the voltage range of 1.5−3.85 V on the LAND testing system, and the specific capacity was calculated based on the weight of the MnO_2 phase.

3. RESULTS AND DISCUSSION

3.1. Structure of 3D Graphene/MnO_2 Hybrids. Figure 1a illustrates the preparation process of 3D graphene/MnO_2 hybrids. First of all, 3D graphene was one-step hydrothermally synthesized in the homogeneous GO−EDA suspension. The as-prepared 3D graphene exhibits a typical porous monolithic structure with a large surface area of 259 m^2/g (nitrogen adsorption/desorption isotherm is shown in Figure S1m, Supporting Information). It makes it serve as a perfect substrate for the loading of MnO_2. To this end, this 3D graphene was immersed in acidic $KMnO_4$ solution with a temperature of 80 °C for the bath deposition of δ-MnO_2.

After the bath deposition of MnO_2, as-obtained graphene/MnO_2 hybrids still maintain the 3D monolithic structure. Figure 2a shows the photographs of the initial 3D graphene and the final 3D graphene/MnO_2-60. It is clearly observed that the size and color of the 3D graphene sample become smaller and darker after depositing MnO_2. Nitrogen adsorption/desorption measurement of the 3D graphene/MnO_2-60 shows that it has a high BET surface area of 218 m^2/g (see Figure S1, Supporting Information), indicating that the addition of MnO_2 does not remarkably decrease the surface area of the initial 3D graphene. Moreover, the 3D graphene/MnO_2-60 sample can endure a weight of 20 g without any damage and deformation (see Figure S2, Supporting Information), exhibiting the desirable strength property. The morphologies of as-prepared graphene/MnO_2 hybrids with the different growth times were studied by SEM, and Figure 2b−f shows the corresponding SEM images. At the beginning, discrete MnO_2 particles appear on the surfaces of graphene sheets and these particle-like MnO_2 would serve as the seeds/nuclei for the further growth of MnO_2. As a consequence, with the increase of reaction time, flower-like MnO_2 nanosheets grow and fully cover all surfaces of the graphene sheets. We postulate that this formation mechanism of flower-like MnO_2 mainly includes two steps: the nucleation process and the growth process. In the acidic condition, the nucleation reaction is as follows:[23]

$$4KMnO_4 + 3C + 4HCl \rightarrow 4MnO_2 + 3CO_2 + 4KCl + 2H_2O \quad (4)$$

With the increase of reaction time, further growth of MnO_2 nanosheets from the initial nuclei occurs as follows:[23]

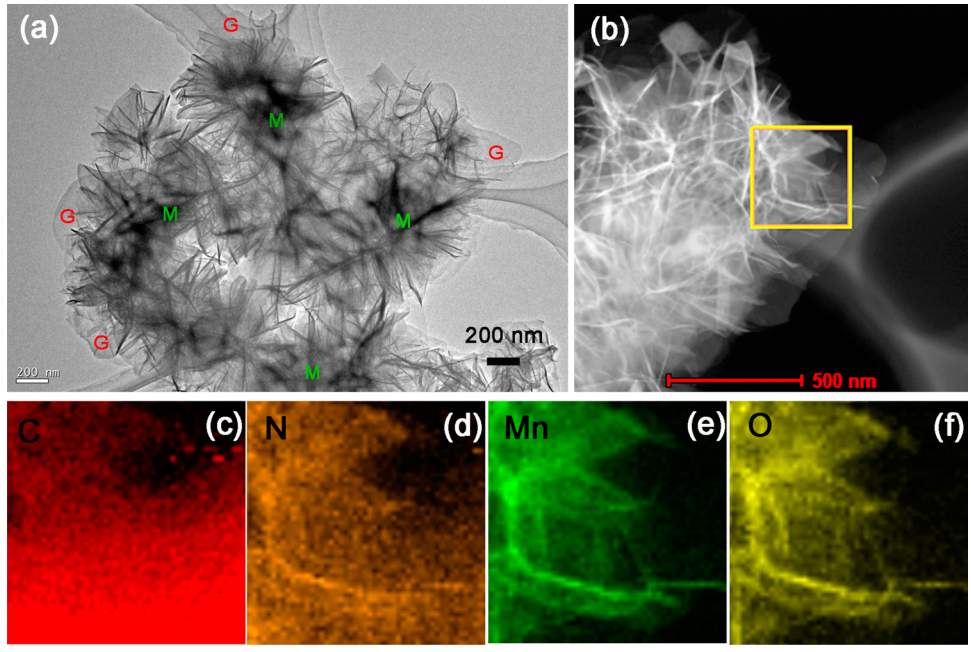

Figure 3. (a) TEM image of 3D graphene/MnO_2-60 (graphene sheets are marked in red and MnO_2 sheets are marked in green), (b) typical STEM image and (c–f) corresponding elemental mapping images taken from the square region marked in (b): (c) C, (d) N, (e) Mn and (f) O.

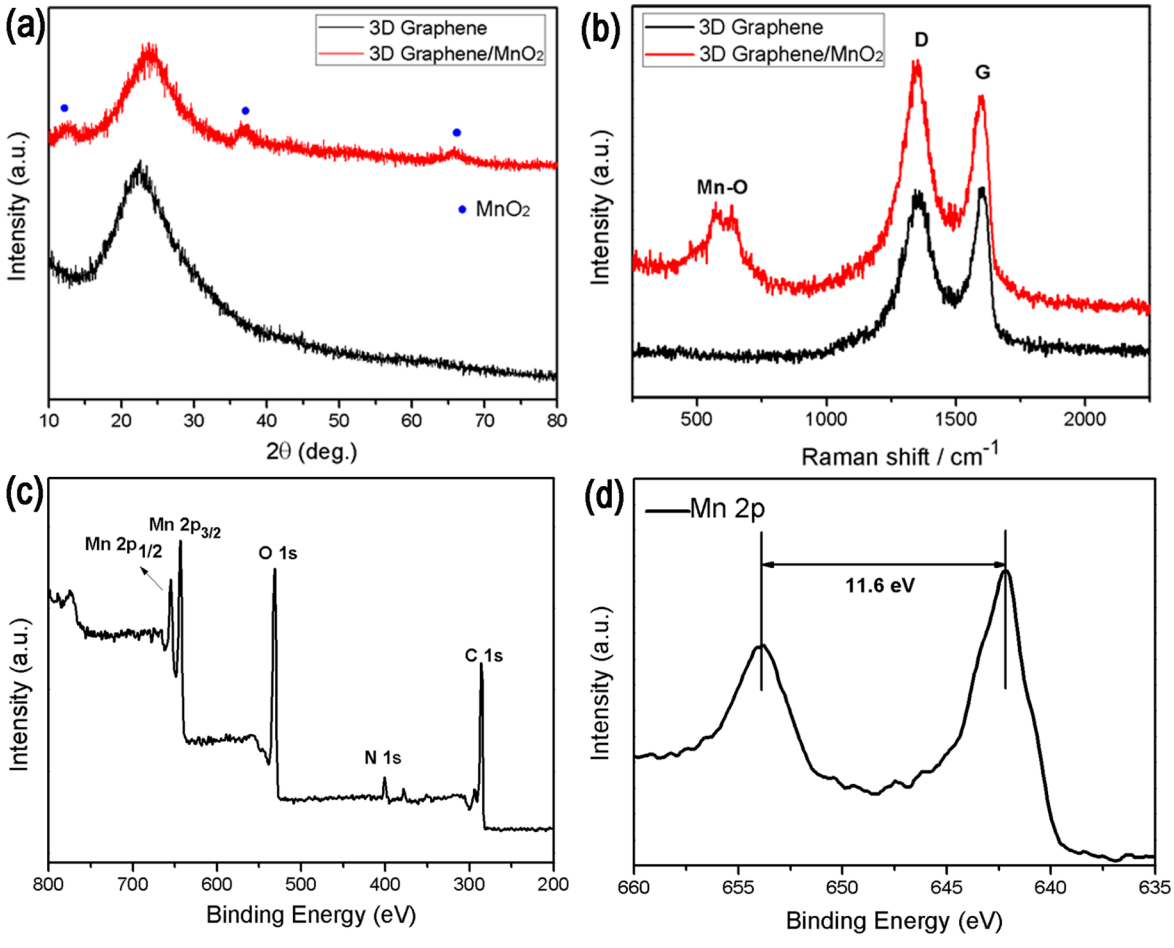

Figure 4. (a) XRD patterns of 3D graphene and 3D graphene/MnO_2-60. (b) Raman spectra of 3D graphene and 3D graphene/MnO_2-60. (c) XPS spectrum of 3D graphene/MnO_2-60. (d) Mn 2p XPS spectrum of 3D graphene/MnO_2-60.

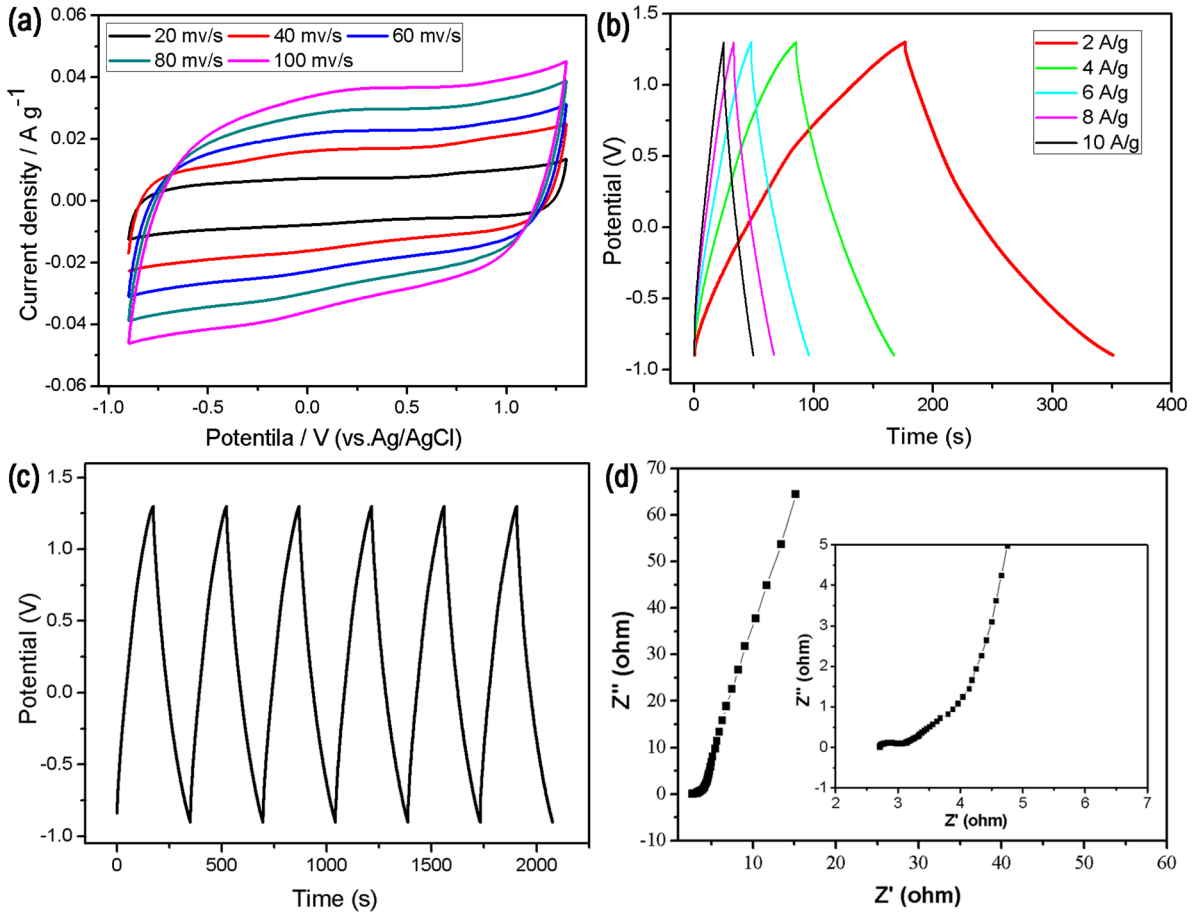

Figure 5. (a) CVs of the 3D graphene/MnO_2-60 at scan rates of 20, 40, 60, 80 and 100 mV/s. (b) GCD curves of the 3D graphene/MnO_2-60 at different current densities and (c) at a constant current of 2 A/g. (d) Nyquist plot of the 3D graphene/MnO_2-60. Inset: the data in the region of high frequencies.

$$4KMnO_4 + 2H_2O \rightarrow 4MnO_2 + 4KOH + 3O_2 \quad (5)$$

TEM and X-ray elemental mappings were performed to further study the 3D graphene/MnO_2. As shown in Figure 3a,b, it is observed that many nanosheets are very thin and uniformly cover the surfaces of graphene sheets. Also, the corresponding elemental mapping images (Figure 3c,d,e,f) further suggest that MnO_2 nanosheets are coated on the graphene. It should be mentioned that, during the preparation of the TEM specimen, MnO_2 nanosheets are still incorporated on the surfaces of graphene sheets and not peeled off after a sonication process (the integral structure of 3D graphene has been destroyed in this process), implying the strong interaction between MnO_2 nanosheets and graphene sheets. In addition, the appearance of N comes from EDA.[3] That is to say, the 3D graphene in this system is virtually N-doping 3D graphene.

The XRD patterns for the 3D graphene and 3D graphene/MnO_2 are included for comparison, as shown in Figure 4a. For 3D graphene, an observed broad diffraction peak at ca. 23° can be indexed to the (002) reflection of graphitic carbon (JCPDS 75-1621). For the graphene/MnO_2-60 sample, except for the characteristic reflection from graphene, three broad peaks around 12°, 37° and 66° can be indexed to the monoclinic lamellar structure of birnessite-type MnO_2 (JCPDS 42-1317)[24,25] Raman spectra of 3D graphene and 3D graphene/MnO_2-60 are listed in Figure 4b. The D band at 1358 cm^{-1} and the G band at 1511 cm^{-1} reveal the presence of graphene. New prominent peaks at 571 and 633 cm^{-1} appear in the spectrum of 3D graphene/MnO_2-60, which are usually attributed to the (Mn−O) stretching vibration and the symmetric stretching vibration in the basal plane of MnO_6 sheet.[26,27] Moreover, the XPS full spectrum also reveals the existence of Mn, O, C and N (Figure 4c). The Mn $2p_{3/2}$ peak is centered at 642.1 eV and Mn $2p_{1/2}$ peak at 653.7 eV with a spin-energy separation of 11.6 eV (Figure 4d), which agree well with those reported for MnO_2, indicating the 4^+ oxidation state for Mn.[28] In addition, it should be mentioned that the amounts of MnO_2 in 3D graphene/MnO_2 hybrids can easily be controlled by the reaction time. By XPS and EA analyses, the mass percentages of MnO_2 in 3D graphene/MnO_2 hybrids with the reaction time of 10, 30, 60 and 120 min are ~13, 22, 59 and 73 wt %, respectively.

3.2. Application in Supercapacitor. In our study, as-prepared 3D graphene/MnO_2 hybrids can be directly pressed into nickel foams as binder-free working electrodes, and their electrochemical capacitive properties in 2 M $EMIMBF_4$/AN electrolyte were systematically investigated. First, the cyclic voltametry (CV) scans of the different 3D graphene/MnO_2 hybrid electrodes were performed at scans rates of 50 mv/s, and the corresponding curves are shown in Figure S3 (Supporting Information). The results show that the amount of MnO_2 is crucial to electrochemical capacitance. Among the four different 3D graphene/MnO_2 hybrids, the 3D graphene/MnO_2-60 sample displays the largest area of CV profile. It also can be seen that there is no obvious difference in the CVs between the 3D graphene/MnO_2-30 and the 3D graphene/MnO_2-120, indicating that the overhigh mass loading would lead to the decrease of the specific capacitance due to the close-packed structure resulting in limited electrochemically active surface area, so only

dx.doi.org/10.1021/am5024258 | ACS Appl. Mater. Interfaces 2014, 6, 11665−11674

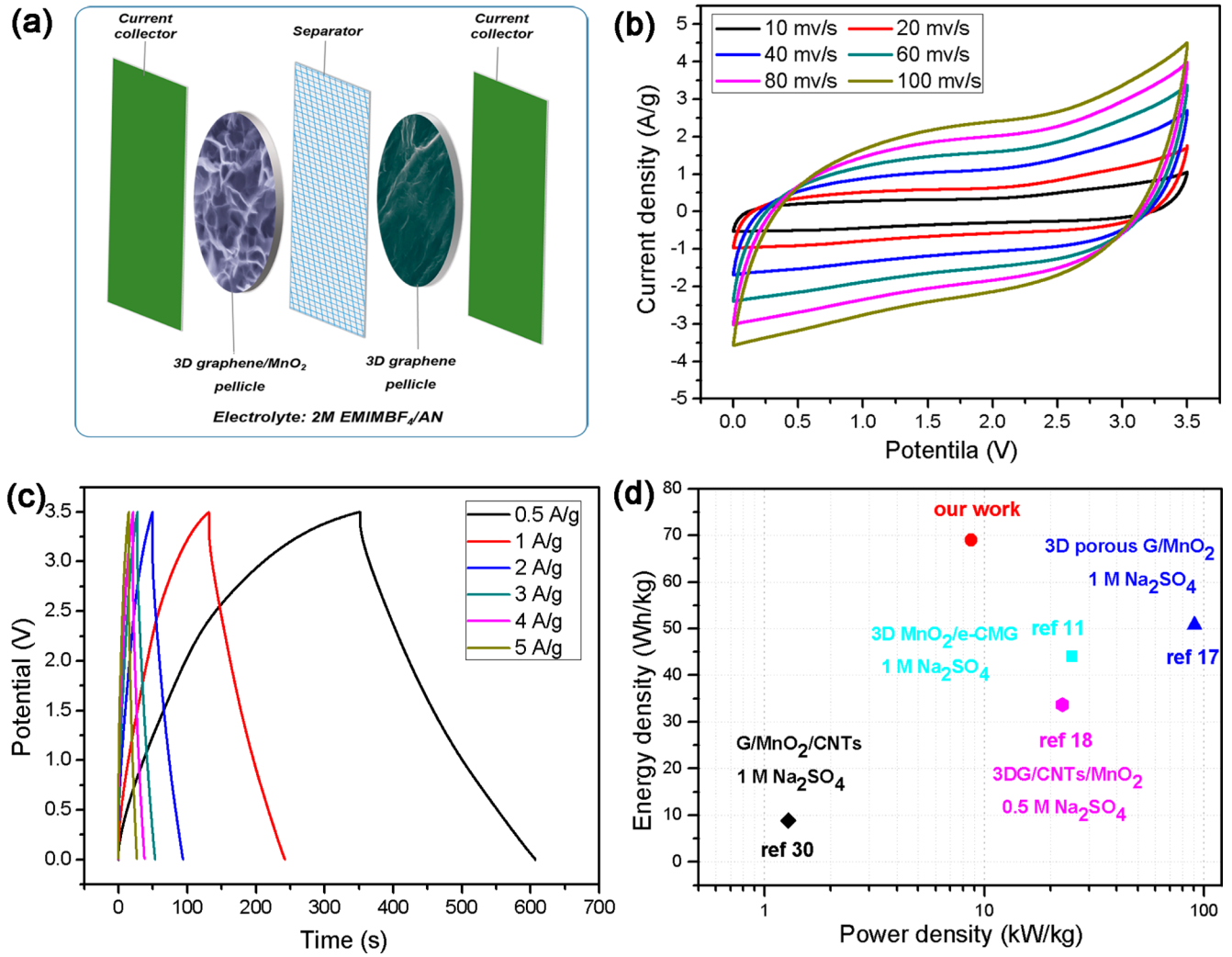

Figure 6. (a) Schematic of the structure of as-made asymmetric supercapacitor consisting of 3D graphene/MnO_2-60 and 3D graphene electrodes, a separator, and two current collectors. (b) CVs of the asymmetric supercapacitor at different scan rates. (c) GCD curves of the asymmetric supercapacitor at different current densities. (d) Ragone plots of the asymmetric supercapacitor compared with the values of similar asymmetrical systems from refs 11, 17, 18 and 30.

appropriate amount of MnO_2 can deliver high specific capacitance.[29] The CV and galvanostatic charging/discharging (GCD) curves of pure 3D graphene in a three-electrode system are shown in Figure S4 (Supporting Information). It is achieving a high specific capacitance of 150 F/g at 1 A/g.

Figure 5a shows the rate-dependent CVs for the sample 3D graphene/MnO_2-60 with the scan rates range of 20−100 mV/s. It can be seen that the 3D graphene/MnO_2-60 electrode shows a relatively rectangular CV curve, indicating a nearly ideal supercapacitor behavior. Furthermore, as the scan rate increases, the shapes of CV curves do not change significantly, suggesting a good rate capability. Its GCD curves at different current densities over the voltage window of 0.9−1.3 V are shown in Figure 5b. Also, Figure 5c shows the cycling charge/discharge curves at a constant current density of 2 A/g. As the curves show, the 3D graphene/MnO_2-60 electrode presents approximate symmetric charge/discharge curves and good capacitive behavior with a rapid $I-V$ response. At same time, it is achieving high-capacitance performance with the specific capacitance up to 236 F/g at 0.25 A/g. The enhanced electrochemical performance of the 3D graphene/MnO_2-60 electrode is further conformed by EIS and the resulting Nyquist plots are shown in Figure 5d. Two parts composed of Warburg arc in the high frequency region and a straight slopping line in the middle-to-low frequency region can be observed in this sample. In the low-frequency region, the diffusing line comes close to an ideal straight line along the imaginary axis, which is a characteristic feature of capacitive behavior. In the high-frequency intercept of the real axis, an internal resistance (R_s) can be observed, which includes the resistance of the electrolyte and the intrinsic resistance of the electrode material. As seen from the enlarged image in the inset, the small semicircle indicates the low charge-transfer resistance (R_{ct}), which results from the high electrical conductivity of the 3D graphene framework and the uniform dispersion of the MnO_2 nanosheets.

To explore the advantage of such 3D graphene/MnO_2-60 hybrids for real applications, an asymmetric supercapacitor device was prepared by assembling 3D graphene/MnO_2-60 as the positive electrode and 3D graphene as the negative electrode in 2 M $EMIMBF_4$/AN electrolyte, as shown in Figure 6a. The symmetry rectangular shapes of the CV curves indicate its ideal pseudocapacitive nature, even at a high scan rate of 100 mV/s (Figure 6b). As the GCD curves show (Figure 6c), the linear voltage versus time profiles reveal good capacitive characteristics

dx.doi.org/10.1021/am5024258 | ACS Appl. Mater. Interfaces 2014, 6, 11665−11674

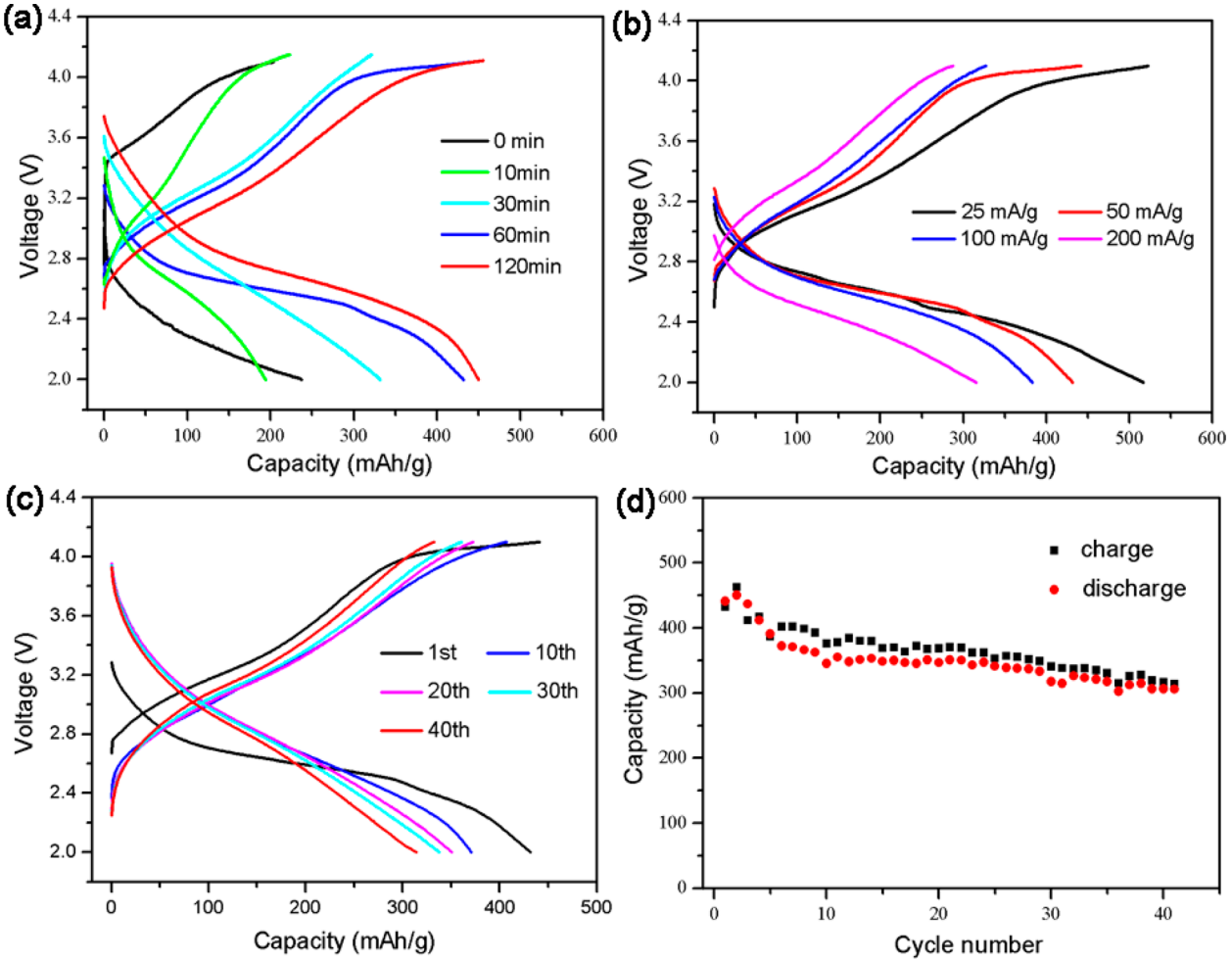

Figure 7. (a) Charging–discharging curves of 3D graphene and 3D graphene/MnO_2 hybrids prepared with different reaction times at a current density of 50 mA/g. (b) Rate property of 3D graphene/MnO_2-60 at various current densities between 2.0 and 4.1 V. (c and d) Corresponding cycling performance of 3D graphene/MnO_2-60 electrode at a current density of 50 mA/g.

for our supercapacitor. Moreover, the series resistance of the device is ~2.7 Ω, as determined from the Nyquist plot in Figure S5 (Supporting Information), indicating a low internal resistance for the whole device. The cycling stability is a critically important characteristic for an asymmetric supercapacitor. As shown in Figure S6 (Supporting Information), after 1000 charging/discharging cycles, the capacitance retention rates remained over 80%. The decay is mainly due to the relatively poor stability of MnO_2 in ionic liquid electrolyte.

In addition, the power and energy density values of the supercapacitor device were evaluated by the galvanostatic charge/discharge curves. As shown in Figure 6d, Ragone plot of the relation E and P shows the maximum energy and power density of 68.4 Wh/kg and 8.79 kW/kg, respectively. The energy density value is higher than those of 3D MnO_2/e-CMG, 3DG/CNTs/MnO_2, 3D porous G/MnO_2 and G/MnO_2/CNTs materials[11,17,18,30] As we know, the energy density of a supercapacitor is proportional to the square of cell voltage. The operating cell voltage of our supercapacitor device in ionic liquid electrolyte can be extended to 3.5 V, consequently resulting in a great increase in energy density.

3.3. Application in Li–O_2 Battery. Here, the Li–O_2 battery, containing a 3D graphene/MnO_2-based O_2 catalytic electrode (positive) and a Li-electrode (negative) in 1 M $LiCF_3SO_3$/TEGDME electrolyte was constructed as described in the section 2. Figure 7a performs the discharge/charge curves of the 3D graphene and 3D graphene/MnO_2 hybrid electrodes with different reaction times (10, 30, 60 and 120 min) at a current density of 50 mA/g. The pure 3D graphene Li–O_2 battery has a limited discharge capacity of 236 mAh/g. However, it is interesting to find that the Li–O_2 battery using 3D graphene/MnO_2-10 displays an approximate discharge capacity to that of the pure 3D graphene, but obviously a lower initial voltage for both charge and discharge. The low capacity would be attributed to the low crystallinity and the low content of MnO_2 in the 3D graphene/MnO_2-10 sample. Increasing the reaction time of 3D graphene/MnO_2 (to 30, 60 and 120 min) results in the gradually increased capacity values. For instance, 3D graphene/MnO_2-120 displays a discharge capacity of 450 mAh/g, indicating that it can effectively facilitate the oxygen reduction reaction (ORR) during the discharge process. Moreover, all 3D graphene/MnO_2 electrodes exhibit excellent oxygen evolution reaction (OER) catalytic performance for the low medium voltage in charging process. The medium voltages of the 3D graphene/MnO_2-x hybrids (x = 10, 30, 60 or 120) in the charging process are 3.52, 3.44, 3.53 and 3.46 V, respectively. Simultaneously, the medium voltage differences between the charging and discharging processes are 0.93, 0.87, 0.90 and 0.75 V, respectively. But these curves do not show any obvious platforms. This phenomenon can be explained from the reaction principle of a Li–O_2 battery. The electrode reaction

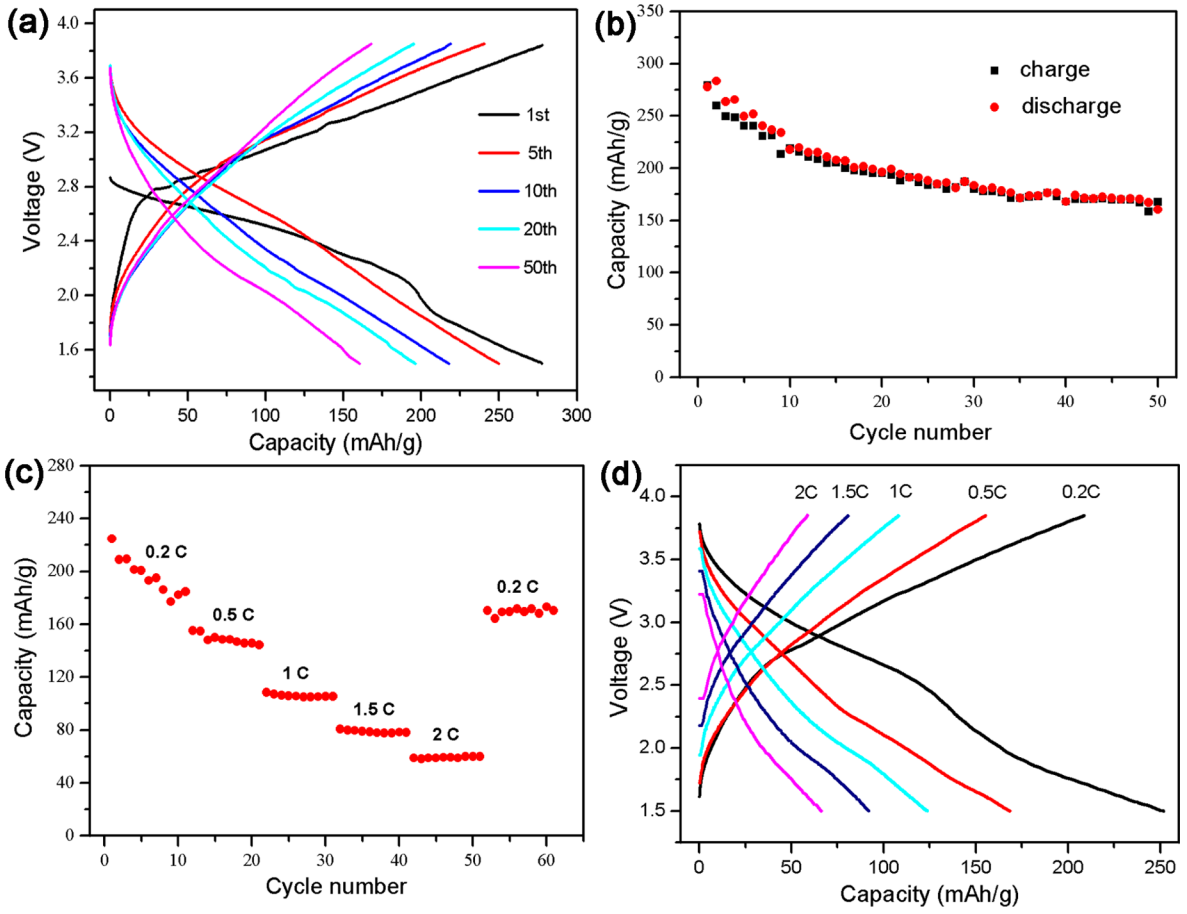

Figure 8. (a and b) Cycling performance of 3D graphene/MnO_2-120 showing at a current density of 0.2 C. (c) Rate property of 3D graphene/MnO_2-120 at various current densities. (d) The corresponding charging−discharging curves at different current densities.

on the discharge/charge process has already been summarized as the equation $O_2 + 2Li^+ + 2e^- \rightarrow Li_2O_2$.[31] According to the equation, O_2 is reduced into Li_2O_2 on the discharge process. With the increased deposition of the Li_2O_2 during the discharge, a well-known insulator, the impedance of the electrode becomes more and more large, which will further lead to higher polarization. In addition, Li_2O_2 mainly deposits on the O_2-facing side for the 3D cathode,[32] which increases the contact impedance between the electrode and the cathode shell to some extent. Figure 7b shows the discharge/charge curves of the 3D graphene/MnO_2-60 sample used in Li−O_2 battery at different current densities. It can deliver the capacity of 517, 432, 384 and 316 mAh/g at 25, 50, 100 and 200 mA/g, respectively. The results demonstrate that the as-prepared hybrid cathode exhibits excellent catalytic performance for both ORR and OER even at high current densities. Cycle performance of this Li−O_2 battery at a current density of 50 mA/g is shown in Figure 7c,d. It can be observed that the discharge capacity still remains at 314 mAh/g after 40 cycles with 72.7% of its initial specific capacity. It has been reported that considerable improvement of the cyclability can be achieved by controlling the discharge and charge protocol of the Li−O_2 cells, i.e., limiting the depth of the discharge.[33] However, the 3D graphene/MnO_2-60 hybrid cathode still shows superior cycle performance at the window between 2.0 and 4.1 V without any limitations.

The satisfactory results may be due to the unique structure and mechanical strength of the 3D graphene/MnO_2. The 3D conductive network facilitates the transfer of electrons, which is the premise for the complete decomposition of Li_2O_2 on charge. Meanwhile, the considerable mechanical strength can prevent the damage of the three-dimensional structure from the deposition of Li_2O_2 during the discharge.[34]

3.4. Application in Li−MnO_2 Battery. Here, the as-prepared 3D graphene/MnO_2-120 hybrid with the maximum MnO_2 loading (about 73 wt %) was employed as the cathode for the Li−MnO_2 battery. The cell was cycled within the potential window from 1.5 to 3.85 V (vs Li/Li^+) at 0.2 C (the theoretical capacity of the MnO_2 is 308 mAh/g). Figure 8a gives the corresponding discharge/charge curves at the selected cycle numbers (1st, 5th, 10th, 20th and 50th). A discharge capacity of 275 mAh/g is obtained for the first cycle, which decreases to a value of 249, 218, 196 and 160 mAh/g at the 5th, 10th, 20th and 50th cycle numbers, respectively. Figure 8b shows almost steady capacities (around 165 mAh/g) after 30 cycles and high Coulombic efficiency for the nearly consonant capacities between charge and discharge. This result indicates that the 3D graphene framework is an ideal carbon matrix for anchoring MnO_2 nanosheets. Moreover, the rate capability of 3D graphene/MnO_2-120 cathode was also tested and the corresponding results are shown in Figure 8c,d. Although the discharge capacity decreases along with the increase of current density, the cell still delivers a stable capacity at high rates, even at 2 C. In addition, it should be noticed that as long as the current rate reverses a low current rate (0.2 C), the specific capacity can recover to the original value (about 172 mAh/g), indicating that the integrity of the 3D graphene/MnO_2-120 hybrid cathode is

well maintained. Therefore, the 3D graphene/MnO_2-120 is a promising cathode material for Li−MnO_2 batteries owning to its efficiently conductive network and its structure stability.

4. CONCLUSIONS

We have developed a type of free-standing 3D graphene/MnO_2 hybrids as binder-free electrodes for supercapacitors and Li−O_2 and Li−MnO_2 batteries. The results show that our 3D graphene/MnO_2 is an ideal binder-free electrode material for energy and catalytic applications. The unique structure of the 3D graphene/MnO_2 hybrids facilitates electron transfer, as shown in Figure 1b. The main reasons can be ascribed as follows: (a) with the 3D backbone of 3D graphene, it is facile to obtain 3D graphene/MnO_2 hybrid structures that dramatically increase the surface area of the MnO_2 component and efficiently promote the formation of interconnected mesopores within the 3D frameworks. The high active surface area and interconnected mesopores are favorable to ion diffusion from the external electrolyte to the interior surfaces. (b) The conductive graphene sheets within the 3D frameworks can serve as thin layer current collectors and multidimensional pathways to facilitate the transport of electrons in the bulk electrode and the electrical connection of the MnO_2 nanosheets with the graphene frameworks. (c) The flower-like architecture of deposited MnO_2 nanosheets has a larger specific surface area and higher surface-to-bulk ratio than one-dimensional MnO_2 structures, which can offer abundant electrochemically active surface areas for charge transfer and reduce ion diffusion length during the charge/discharge process. (d) During the formation process of flower-like MnO_2, graphene sheets would first react with $KMnO_4$ for the MnO_2 nucleation. Thus, in the final 3D graphene/MnO_2 hybrid, the MnO_2 nanosheets are uniformly anchored on the 3D graphene framework with strong adhesion. Such a strong interaction is also favorable to the charge transfer during the charging/discharging process.

■ ASSOCIATED CONTENT

Supporting Information

Nitrogen adsorption/desorption isotherms of 3D graphene and 3D graphene/MnO_2-60 samples, photograph of the freestanding sample, CVs of the 3D graphene and 3D graphene/MnO_2 hybrids prepared with different reaction times and Nyquist plot of the asymmetric supercapacitor. This material is available free of charge via the Internet at http://pubs.acs.org.

■ AUTHOR INFORMATION

Corresponding Author

*Prof. Xingbin Yan. Fax: (+86) 931 4968055. E-mail: xbyan@licp.cas.cn.

Author Contributions

⊥The paper was written through contributions of all authors. All authors have given approval to the final version of the paper. These authors (Xiaoli Zhu; Peng Zhang) contributed equally.

Funding

National Nature Science Foundations of China (21103205, 21203223 and 21303234)

Notes

The authors declare no competing financial interest.

■ ACKNOWLEDGMENTS

This work was supported by the National Nature Science Foundations of China (21103205, 21203223 and 21303234).

■ REFERENCES

(1) Li, C.; Shi, G. Q. Three-Dimensional Graphene Architectures. *Nanoscale* **2012**, *4*, 5549−5563.

(2) Xu, Y. X.; Sheng, K. X.; Li, C.; Shi, G. Q. Self-Assembled Graphene Hydrogel via a One-Step Hydrothermal Process. *ACS Nano* **2011**, *4*, 4324−4330.

(3) Hu, H.; Zhao, Z. B.; Wan, W. B.; Gogotsi, Y.; Qiu, J. S. Ultralight and Highly Compressible Graphene Aerogels. *Adv. Mater.* **2013**, *25*, 2219−2223.

(4) Wu, Z. S.; Winter, A.; Chen, L.; Sun, Y.; Turchanin, A.; Feng, X.; Müllen, K. Three-Dimensional Nitrogen and Boron Co-doped Graphene for High-Performance All-Solid-State Supercapacitors. *Adv. Mater.* **2012**, *24*, 5130−5135.

(5) Zhang, L.; Shi, G. Q. Preparation of Highly Conductive Graphene Hydrogels for Fabricating Supercapacitors with High Rate Capability. *J. Phys. Chem. C* **2011**, *115*, 17206−17212.

(6) Zhu, Y. W.; Murali, S.; Stoller, M. D.; Ganesh, K. J.; Cai, W. W.; Ferreira, P. J.; Pirkle, A.; Wallace, R. M.; Cychosz, K. A.; Thommes, M.; Su, D.; Stach, E. A.; Ruoff, R. S. Carbon-Based Supercapacitors Produced by Activation of Graphene. *Science* **2011**, *332*, 1537−1541.

(7) Li, N.; Chen, Z. P.; Ren, W. C.; Li, F.; Cheng, H. M. Flexible Graphene-based Lithium Ion Batteries with Ultrafast Charge and Discharge Rates. *Proc. Natl. Acad. Sci. U. S. A.* **2012**, *109*, 17360−17365.

(8) Zhang, W. Y.; Zhu, J. X.; Ang, H. X.; Zeng, Y.; Xiao, N.; Gao, Y. B.; Liu, W. L.; Hng, H. H.; Yan, Q. G. Binder-Free Graphene Foams for O_2 Electrodes of Li-O_2 Batteries. *Nanoscle* **2013**, *5*, 9651−9658.

(9) Chen, R. J.; Zhao, T.; Lu, J.; Wu, F.; Li, L.; Chen, J. Z.; Tan, G. Q.; Ye, Y. S.; Amine, K. Graphene-Based Three-Dimensional Hierarchical Sandwich-Type Architecture for High-Performance Li/S Batteries. *Nano Lett.* **2013**, *13*, 4642−4649.

(10) Zhao, S. L.; Yin, H. J.; Du, L.; Yin, G. P.; Tang, Z. Y.; Liu, S. Q. Three Dimensional N-Doped Graphene/PtRu Nanoparticle Hybrids as High Performance Anode for Direct Methanol Fuel Cells. *J. Mater. Chem. A* **2014**, *2*, 3719−3724.

(11) Choi, B. G.; Yang, M. H.; Hong, W. H.; Choi, J. W.; Huh, Y. S. 3D Macroporous Graphene Frameworks for Supercapacitors with High Energy and Power Densities. *ACS Nano* **2012**, *6*, 4020−4028.

(12) Xu, Y. X.; Huang, X. Q.; Lin, Z. Y.; Zhong, X.; Huang, Y.; Duan, X. F. One-Step Strategy to Graphene/$Ni(OH)_2$ Composite Hydrogels as Advanced Three-Dimensional Supercapacitor Electrode Materials. *Nano Res.* **2012**, *6*, 65−76.

(13) Cao, Y.; Wei, Z. K.; He, J.; Zang, J.; Zhang, Q.; Zheng, M. S.; Dong, Q. F. α-MnO2 Nanorods Grown in Situ on Graphene as Catalysts for Li−O_2 Batteries with Excellent Electrochemical Performance. *Energy Environ. Sci.* **2012**, *5*, 9765−9768.

(14) Chen, Y.; Prasad, K. P.; Wang, X. W.; Pang, H. C.; Yan, R. Y.; Than, A.; Chan-Park, M. B.; Chen, P. Enzymeless Multi-Sugar Fuel Cells with High Power Output Based on 3D Graphene−Co_3O_4 Hybrid Electrodes. *Phys. Chem. Chem. Phys.* **2013**, *15*, 9170−9176.

(15) Wu, Z. S.; Yang, S. B.; Sun, Y.; Parvez, K.; Feng, X. L.; Mullen, K. 3D Nitrogen-Doped Graphene Aerogel-Supported Fe_3O_4 Nanoparticles as Efficient Electrocatalysts for the Oxygen Reduction Reaction. *J. Am. Chem. Soc.* **2012**, *134*, 9082−9085.

(16) Gong, Y. J.; Yang, S. B.; Liu, Z.; Ma, L. L.; Vajtai, R.; Ajayan, P. M. Graphene-Network-Backboned Architectures for High-Performance Lithium Storage. *Adv. Mater.* **2013**, *25*, 3979−3984.

(17) Shao, Y. L.; Wang, H. Z.; Zhang, Q. H.; Li, Y. G. High-Performance Flexible Asymmetric Supercapacitors Based on 3D Porous Graphene/MnO_2 Nanorod and Graphene/Ag Hybrid Thin-Film Electrodes. *J. Mater. Chem. C* **2013**, *1*, 1245−1251.

(18) Chen, W. J.; He, Y. M.; Li, X. D.; Zhou, J. Y.; Zhang, Z. X.; Zhao, C. H.; Gong, C. S.; Li, S. K.; Pan, X. J.; Xie, E. Q. Facilitated Charge Transport in Ternary Interconnected Electrodes for Flexible Supercapacitors with Excellent Power Characteristics. *Nanoscale* **2013**, *5*, 11733−11741.

(19) Tu, F. Y.; Wu, T. H.; Liu, S. Q.; Jin, G. H.; Pan, C. Y. Facile Fabrication of MnO_2 Nanorod/Graphene Hybrid as Cathode Materials for Lithium Batteries. *Electrochim. Acta* **2013**, *106*, 406−410.

(20) Hummers, W. S.; Offeman, R. E. Preparation of Graphitic Oxide. *J. Am. Chem. Soc.* **1958**, *80*, 1339−1341.
(21) Zhang, X.; Zhao, D. D.; Zhao, Y. Q.; Tang, P. Y.; Shen, Y. L.; Xu, C. L.; Li, H. L.; Xiao, Y. High Performance Asymmetric Supercapacitor Based on MnO_2 Electrode Inionic Liquid Electrolyte. *J. Mater. Chem. A* **2013**, *1*, 3706−3712.
(22) Wu, Z. S.; Ren, W. C.; Wang, D. W.; Li, B. L.; Cheng, H. M. High-Energy MnO_2 Nanowire/Graphene and Graphene Asymmetric Electrochemical Capacitors. *ACS Nano* **2010**, *4*, 5835−5842.
(23) Dong, X. C.; Wang, X. W.; Wang, J.; Song, H.; Li, X. G.; Wang, L. H.; Chan-Park, M. B.; Li, C. M.; Chen, P. Synthesis of a MnO_2−Graphene Foam Hybrid with Controlled MnO_2 Particle Shape and Its Use as a Supercapacitor Electrode. *Carbon* **2012**, *50*, 4865−4870.
(24) Yan, J.; Fan, Z. J.; Wei, T.; Qian, W. Z.; Zhang, M. L.; Wei, F. Fast and Reversible Surface Redox Reaction of Graphene−MnO_2 Composites as Supercapacitor Electrodes. *Carbon* **2010**, *48*, 3825−3833.
(25) Zhu, J. Y.; He, J. H. Facile Synthesis of Graphene-Wrapped Honeycomb MnO_2 Nanospheres and Their Application in Supercapacitors. *ACS Appl. Mater. Interfaces* **2012**, *4*, 1770−1776.
(26) Ma, S. B.; Ahn, K. Y.; Lee, E. S.; Oh, K. H.; Kim, K. B. Synthesis and Characterization of Manganese Dioxide Spontaneously Coated on Carbon Nanotubes. *Carbon* **2007**, *45*, 375−382.
(27) Julien, C.; Massot, M.; Baddour-Hadjean, R.; Franger, S.; Bath, B.; Pereira-Ramos, J. P. Raman Spectra of Birnessite Manganese Dioxides. *Solid State Ionics* **2003**, *159*, 345−356.
(28) Zhao, G. X.; Li, J. X.; Jiang, L.; Dong, H. L.; Wang, X. K.; Hu, W. P. Synthesizing MnO_2 Nanosheets From Graphene Oxide Templates for High Performance Pseudosupercapacitors. *Chem. Sci.* **2012**, *3*, 433−437.
(29) Mao, L.; Zhang, K.; On Chan, H. S.; Wu, J. J. Nanostructured MnO_2/Graphene Composites for Supercapacitor Electrodes: The Effect of Morphology, Crystallinity and Composition. *J. Mater. Chem.* **2012**, *22*, 1845−1851.
(30) Cheng, Y. C.; Lu, S. T.; Zhang, H. B.; Varanasi, C. V.; Liu, J. Synergistic Effects from Graphene and Carbon Nanotubes Enable Flexible and Robust Electrodes for High-Performance Supercapacitors. *Nano Lett.* **2012**, *12*, 4206−4211.
(31) Jung, H. G.; Hassoun, J.; Park, J. B.; Sun, Y. K.; Scrosati, B. An Improved High-Performance Lithium−Air Battery. *Nat. Chem.* **2012**, *4*, 579−585.
(32) Chervin, C. N.; Long, J. W.; Brandell, N. L.; Rolison, D. R. Carbon Nanofoam-Based Cathodes for Li-O_2 Batteries: Correlation of Pore-Solid Architecture and Electrochemical Performance. *ECS Trans.* **2011**, *35*, 33−42.
(33) Xu, D.; Wang, Z. L.; Xu, J. J.; Zhang, L. L.; Zhang, X. B. Novel DMSO-Based Electrolyte for High Performance Rechargeable Li-O_2 Batteries. *Chem. Commun.* **2012**, *48*, 6948−6950.
(34) Guo, Z. Y.; Zhou, D. D.; Dong, X. L.; Qiu, Z. J.; Wang, Y. G.; Xia, Y. G. Ordered Hierarchical Mesoporous/Macroporous Carbon: A High-Performance Catalyst for Rechargeable Li-O_2 Batteries. *Adv. Mater.* **2013**, *25*, 5668−5672.